Evolutionary paths to antibiotic resistance under dynamically sustained drug selection

Erdal Toprak[1,6], Adrian Veres[2,6], Jean-Baptiste Michel[1,3], Remy Chait[1], Daniel L Hartl[4] & Roy Kishony[1,5]

Antibiotic resistance can evolve through the sequential accumulation of multiple mutations[1]. To study such gradual evolution, we developed a selection device, the 'morbidostat', that continuously monitors bacterial growth and dynamically regulates drug concentrations, such that the evolving population is constantly challenged[2–5]. We analyzed the evolution of resistance in *Escherichia coli* under selection with single drugs, including chloramphenicol, doxycycline and trimethoprim. Over a period of ~20 days, resistance levels increased dramatically, with parallel populations showing similar phenotypic trajectories. Whole-genome sequencing of the evolved strains identified mutations both specific to resistance to a particular drug and shared in resistance to multiple drugs. Chloramphenicol and doxycycline resistance evolved smoothly through diverse combinations of mutations in genes involved in translation, transcription and transport[3]. In contrast, trimethoprim resistance evolved in a stepwise manner[1,6], through mutations restricted to the gene encoding the enzyme dihydrofolate reductase (*DHFR*)[7,8]. Sequencing of *DHFR* over the time course of the experiment showed that parallel populations evolved similar mutations and acquired them in a similar order[9].

Antibiotic resistance is a growing global public health concern[10–12]. Bacteria can acquire resistance via horizontal gene transfer or spontaneous mutation[3,12–14]. Evolution of resistance through the acquisition of single spontaneous mutations is particularly relevant for certain drugs, such as quinolones and rifamycin, for which high-level resistance can result from a single point mutation[15,16]. For most antibiotics, however, multiple mutations are required to develop high levels of resistance[1,6,17,18]. Systematic experimental methods to study the evolution of resistance at the genomic level have been lacking. Although mutational trajectories resulting in particular phenotypes have been suggested, little is known about the phenotypic and genotypic evolutionary pathways leading to high levels of drug resistance or about their reproducibility among populations evolving in parallel[1,3,6,19].

Laboratory evolution experiments have generated important information about genetic changes underlying multiple phenotypes, including drug resistance[3,9,19–23]. In such experiments, bacterial populations are typically exposed to fixed drug concentrations that are chosen to be high enough to partially or completely inhibit growth of the base strain, thus imposing a selective advantage for resistant mutants, yet low enough for some spontaneously occurring resistant mutants to survive[19,23–25]. The range of drug concentrations that matches these criteria is termed the mutant-selection window (MSW)[26]. The MSW, however, is not fixed; after each strain containing a resistance-conferring mutation becomes dominant in the culture, a higher drug concentration is needed to maintain the selection pressure on the population's now-higher resistance level. The rate at which the inhibitory drug concentration increases, which reflects the rate of evolution of resistance, can vary across evolutionary time and with the use of different drugs. Therefore, an unequivocal comparison of long-term evolution of resistance to different drugs requires experimental methodologies in which the effective drug concentration is continuously tuned according to the actual rate of evolutionary adaptation[2–5,27,28].

We developed a microbial selection device, which we call the morbidostat, that continuously adjusts antibiotic concentration to maintain nearly constant growth inhibition of an evolving microbial population (**Fig. 1a**). Like traditional continuous-culture systems such as chemostats, the morbidostat feeds a culture with fresh medium at a constant rate and bacterial cultures approach a steady state at which the growth rate is equal to the fixed dilution rate. In a chemostat, nutrient limitation provides an inherent feedback that sets the growth rate equal to the dilution rate. In contrast, the growth rate in the morbidostat and similar devices is set by the level of an inhibitor, such as an antibiotic, that is externally adjusted by a control algorithm[2–5,28,29]. The morbidostat maintains the bacterial population at low densities, such that growth is not nutrient limited, and controls the growth rate to match the fixed dilution rate by tuning the antibiotic concentration. Therefore, the morbidostat does not elevate drug concentration in a predefined way but, rather, automatically adjusts drug concentration according to the actual rate at which resistance evolves.

Medium flow and control of drug concentration are implemented in repeated cycles. In each cycle, bacteria grow for a fixed period of time without dilution (Δt = 11 min), throughout which time the

[1]Department of Systems Biology, Harvard Medical School, Boston, Massachusetts, USA. [2]Faculty of Arts and Sciences, Harvard University, Cambridge, Massachusetts, USA. [3]Program for Evolutionary Dynamics, Harvard University, Cambridge, Massachusetts, USA. [4]Department of Organismic and Evolutionary Biology, Harvard University, Cambridge, Massachusetts, USA. [5]School of Engineering and Applied Sciences, Harvard University, Cambridge, Massachusetts, USA. [6]These authors contributed equally to this work. Correspondence should be addressed to R.K. (roy_kishony@hms.harvard.edu).

Received 9 May; accepted 15 November; published online 18 December 2011; doi:10.1038/ng.1034

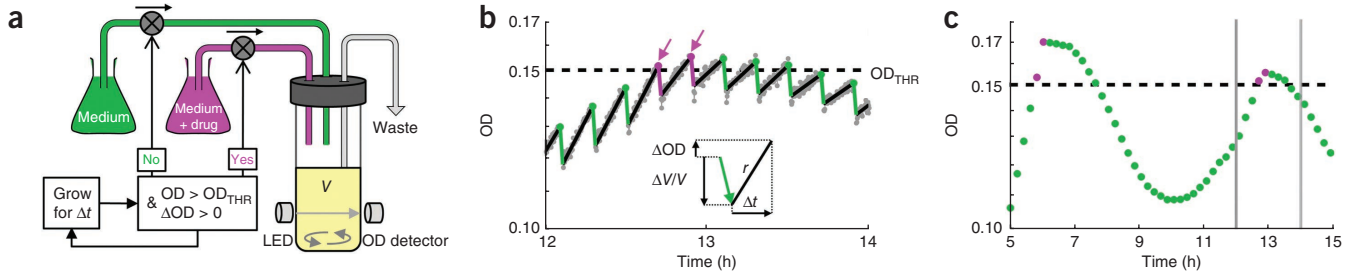

Figure 1 The morbidostat is a continuous-culture device that automatically tunes drug concentration to maintain constant growth inhibition. (**a**) The assay runs in cycles of growth periods (Δt = 11 min) and adds dilutions with either fresh medium (green) or drug solution (magenta). The population is diluted with antibiotic solution when the OD exceeds OD_{THR} (0.15) and the net growth over the complete cycle is positive ($\Delta OD > 0$). (**b**) Representative bacterial growth in the morbidostat. OD is recorded at 1 Hz (plotted at 0.1 Hz, gray dots). The growth rate (r) within a growth period is calculated by fitting the exponential growth function (black lines). Magenta and green markers indicate dilutions with drug solution and fresh medium, respectively. Inset, parameters calculated at each growth cycle are shown. (**c**) Representative bacterial growth and inhibition in the morbidostat for an extended time period. For clarity, only final ODs within growth cycles are plotted. The grey rectangle delimits data shown in **b**. Magenta circles indicate the cycles after the addition of drug solution.

optical density (OD) is recorded **Fig. 1b**, gray dots). The device then calculates the growth rate (r; **Fig. 1b**, black lines) based on the OD measurements and adds a fixed volume ΔV of either medium or drug solution to the culture (**Fig. 1b**,**c**, green and magenta circles, respectively). The drug solution is added only if two conditions are satisfied: (i) the OD is greater than a set threshold ($OD > OD_{THR} = 0.15$) and (ii) the growth rate exceeds the dilution rate ($r > r_{dilution}$, signifying a net increase in OD over the course of the cycle, $\Delta OD > 0$). The parameters ΔV, V and Δt are fixed for the entire experiment and are chosen such that the dilution rate ($r_{dilution} \cong \Delta V / (V \times \Delta t) = 0.4\ h^{-1}$) is equal to half the maximal growth rate in the absence of drug ($r_0 \cong 0.8\ h^{-1}$), forcing the drug concentration to converge to a level at which bacterial growth is inhibited by 50%. Therefore, as bacteria become resistant, drug concentrations are automatically increased to maintain fixed growth inhibition.

Using the morbidostat, we performed an experiment with drug-sensitive *E. coli* (MG1655) in which bacteria were exposed to three antibiotics separately: chloramphenicol, doxycycline and trimethoprim. Chloramphenicol and doxycycline are ribosome inhibitors, and trimethoprim inhibits folic acid biosynthesis by binding to dihydrofolate reductase (DHFR)[8,18,30]. To test the reproducibility of the evolutionary pathways, five isogenic populations (designated as CHL-1–5, DOX-1–5 and TMP-1–5) were evolved in parallel under inhibition by chloramphenicol, doxycycline and trimethoprim, respectively. We followed the evolving dose-response curves of all 15 populations by measuring the growth rates of daily frozen samples of each population over drug concentration gradients (**Fig. 2a**,**b** and Online Methods). These measurements show the evolutionary increase in resistance levels of the populations over time (**Fig. 2b**) (measurements based on drug concentrations and bacterial growth rates recorded during the course of the morbidostat experiment gave similar results for dynamic half-maximal inhibitory concentration (IC_{50}); Online Methods). Note that our IC_{50} calculations are based on exponential growth rate measurements and are therefore insensitive to drug-induced changes in cell size that might affect the conversion of OD to cell number (see **Supplementary Table 1** for the average cell sizes of the ancestral and evolved strains in the presence and absence of drugs).

Over time, the resistance level increased dramatically, with all parallel populations showing similar qualitative and quantitative changes (**Fig. 2**). At the end of the evolution experiments, the IC_{50} values for chloramphenicol, doxycycline and trimethoprim increased by ~870, ~10 and ~1,680 fold, respectively (**Fig. 2c**–**e**). Comparing the evolution pattern for the three drugs, we found that resistance to chloramphenicol and doxycycline increased smoothly over time (**Fig. 2d**,**e**), whereas trimethoprim resistance increased in a stepwise fashion (**Fig. 2b**,**c**). This finding suggests that adaptation to trimethoprim proceeds through adaptive mutations confined to a smaller genomic region, leading to periods of stagnation during which the population awaits the occurrence of rare mutations[31]. To test this hypothesis and

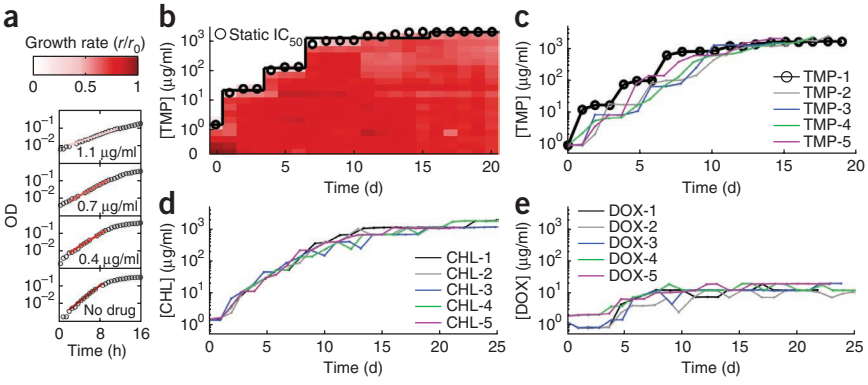

Figure 2 Parallel populations attain high levels of drug resistance in similar adaptive trajectories. (**a**) Sample measurements of OD versus time (circles) and fitted growth rates (exponential fit; color represents normalized growth rate r/r_0) of the ancestral strain in different trimethoprim concentrations. (**b**) Normalized growth rates of bacterial populations obtained from daily samples (x axis) of the evolving populations in a range of fixed drug concentrations (y axis). Day 0 corresponds to the ancestral strain before evolution. IC_{50} values are represented with black circles ($r/r_0 = 0.5$). (**c**–**e**) Resistance levels over time for parallel populations evolving under inhibition by trimethoprim (**c**), chloramphenicol (**d**) and doxycycline (**e**). Resistance increases by ~1,680, 870 and 10 fold, respectively. Trimethoprim resistance increases in a stepwise fashion. The resistance data for each of the 15 populations are derived from high-throughput phenotyping as shown in **a** (the TMP-1 population in **c** (black circles) is the one represented in **b**).

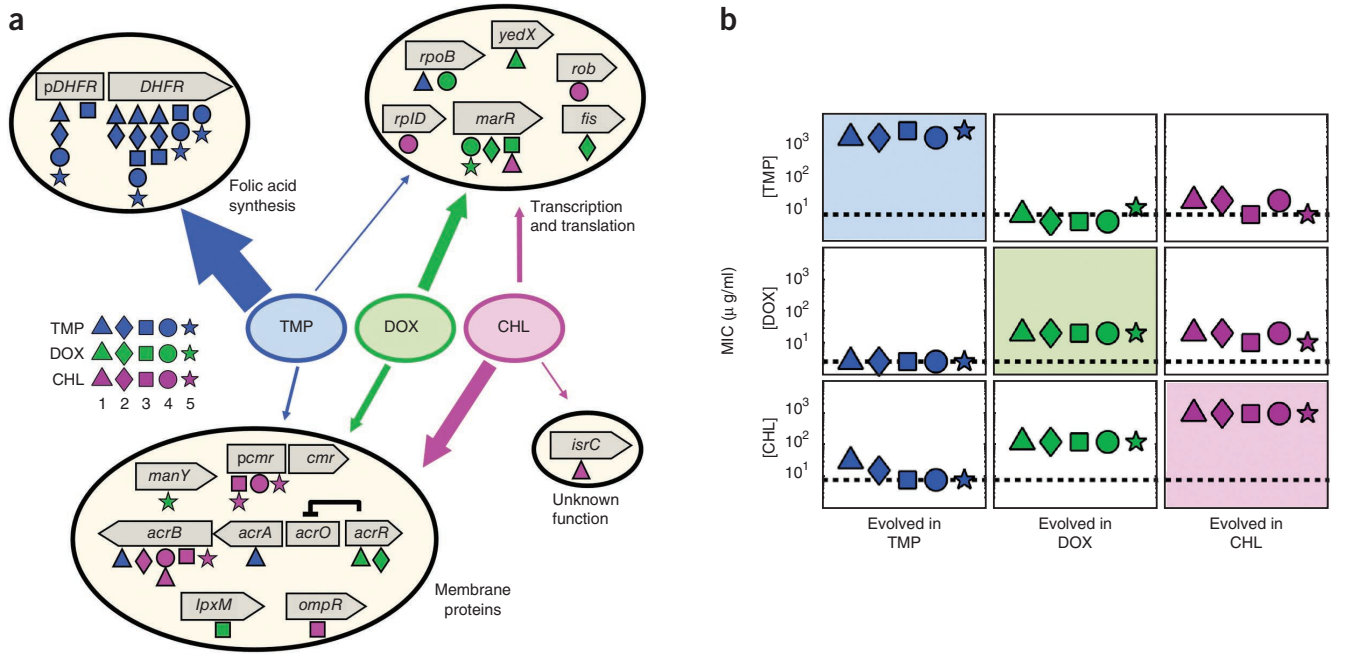

Figure 3 Unique and common genetic changes identified by whole-genome sequencing. (**a**) SNPs identified by Illumina and Sanger sequencing. The horizontal arrow blocks and rectangles represent the coding and noncoding regions of genes, respectively. SNPs found in the 15 evolved populations are shown by different symbols, with colors indicating the drug applied during evolution (magenta, chloramphenicol; green, doxycycline; blue, trimethoprim). Note that SNPs found in multiple populations are shown with vertically stacked symbols appended to the genes. SNPs are localized to genes that fall into three major functional groups: (i) transcription and translation, (ii) folic acid biosynthesis and (iii) membrane transport. Arrow thickness reflects the frequency of mutations occurring within each functional group when the bacterial populations were challenged with the specified drugs. p*DHFR*, *DHFR* promoter; p*cmr*, *cmr* promoter. (**b**) Resistance levels (of Illumina-sequenced clones) to chloramphenicol, doxycycline and trimethoprim. Black dashed lines indicate minimum inhibitory concentration (MIC) for the ancestral strain. Panels with colored background show MIC values for the evolved strains for the drugs to which they evolved resistance. Strains evolved in the presence of chloramphenicol exhibit elevated doxycycline resistance and vice versa, whereas evolution in the presence of trimethoprim inhibition led to little or no cross-resistance for either doxycycline or chloramphenicol.

identify the genetic changes responsible for resistance, we performed whole-genome sequencing of all 15 evolved populations.

We selected an isogenic clone from the final day of the experiment for each evolved population and sequenced their genomes using Illumina whole-genome sequencing (Online Methods). We identified a list of SNPs for each clone and verified them by Sanger sequencing, with ~80% being confirmed (**Supplementary Table 2**). Sequenced strains had two or more SNPs, with the only exception being CHL-2, in which we reliably identified one SNP. **Figure 3a** shows the locations of all 47 SNPs that were found by whole-genome sequencing and confirmed by Sanger sequencing. The majority of these mutations either resulted in amino acid alterations (35 of 47) or were localized to gene promoters (9 of 47). Two silent mutations and a truncating mutation were also observed. Of note, the same silent mutation, g.480645 C>A , was found to have occurred independently in CHL-1 and CHL-4. The clonal abundance of each SNP within the evolving heterogeneous populations was estimated by sequencing each mutated locus in four additional clones derived from the evolved populations. Most SNPs (39 of 47, >75%) were found with high frequency in the populations from which they were isolated (**Supplementary Table 2**). In mapping the coverage of Illumina reads along the genome, we looked for gene deletions and amplifications. Genomic amplifications were found in the CHL-1, DOX-4, DOX-5 and TMP-3 clones, whereas no genomic deletions were detected (**Supplementary Fig. 1**).

Adaptation to drugs inhibiting protein synthesis (chloramphenicol and doxycycline) occurred mostly through mutations in genes encoding membrane proteins and factors involved in transcription or translation (**Fig. 3a**). Mutations found in populations evolved in the presence of these drugs appeared in genes with similar functions as well as in the *acr*, *cmr* and *mar* genes for multidrug resistance known to confer resistance to these antibiotics[17,32,33]. Although doxycycline and chloramphenicol target ribosomes, no mutations were found in ribosomal genes, even though such mutations were previously isolated in selection experiments performed on agar plates[34–37]. The absence of ribosomal mutations may reflect a cost in growth rate or negative epistatic interactions with other mutations fixing in these cultures. Amplified genomic regions in these strains also included multidrug resistance genes or transporter genes. (For example, in the case of *cmr*, one of the populations had an amplification of this gene and others had a promoter mutation; compare CHL-1 with CHL-3–5 in **Supplementary Fig. 1**.) Consistently, all of the populations that evolved resistance to chloramphenicol also developed doxycycline resistance (**Fig. 3b**, middle right panel) and vice versa (**Fig. 3b**, middle bottom panel). For each of these drugs, all of the populations reached the same level of resistance but acquired different sets of mutations (**Fig. 3**). Of note, these populations reached a plateau in their phenotypic adaptation despite the availability of additional mutations conferring drug resistance that occurred in the other populations evolving in parallel. These observations suggest that there are multiple alternative ways to circumvent chloramphenicol- or doxycycline-induced protein synthesis stress, with each requiring a small number of mutations in a diverse set of genes. The waiting time for mutations to appear in these populations is likely to be short due to the large target size for possible mutations, consistent with the smooth phenotypic changes in these populations (**Fig. 2 d**,**e**).

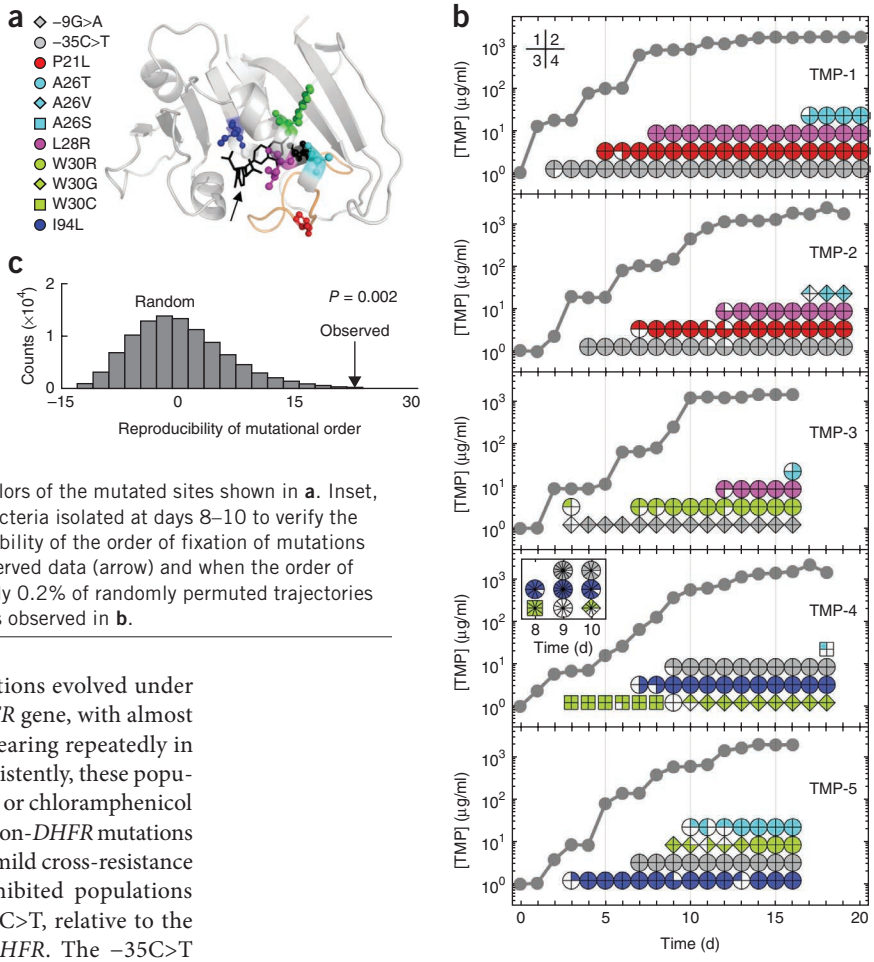

Figure 4 Semi-ordered acquisition of trimethoprim resistance mutations. (**a**) Structure of *E. coli* DHFR enzyme (PDB 1RX2) bound to its substrate, dihydrofolate (black, arrow), with mutated residues shown in color. (**b**) IC_{50} values (gray lines) and time-resolved alterations in DHFR for each of the five replicate (TMP-1–TMP-5). For each day, alterations found in four randomly sampled clones are represented in a pie chart, with color indicating a specific alteration and shape of the chart indicating whether the alteration was a promoter mutation or amino acid substitution. The quadrants of the pie chart indicate the presence (filled) or absence (empty) of this alteration in each of the four sequenced clones (the correspondence between clones and quadrants is conserved across all mutations to indicate whether mutations are found in the same or different clones). Colors of the pie charts correspond to the colors of the mutated sites shown in **a**. Inset, additional colonies (TMP-4) were sequenced from bacteria isolated at days 8–10 to verify the disappearance of the W30C alteration. (**c**) Reproducibility of the order of fixation of mutations compared for the five parallel populations in the observed data (arrow) and when the order of mutations is randomly permuted (histogram bar). Only 0.2% of randomly permuted trajectories are equally or more reproducible than the trajectories observed in **b**.

In contrast, most of the mutations in populations evolved under trimethoprim inhibition were found in the *DHFR* gene, with almost all of the encoded amino acid substitutions appearing repeatedly in several of the parallel evolving populations. Consistently, these populations showed no cross-resistance to doxycycline or chloramphenicol (**Fig. 3b**, left), except for TMP-1, which had three non-*DHFR* mutations in *acrA*, *acrB* and *rpoB* and, accordingly, showed mild cross-resistance to chloramphenicol. All the trimethoprim-inhibited populations acquired one of two mutations (–9G>A or –35C>T, relative to the transcription start site) in the promoter of *DHFR*. The –35C>T mutation is known in a clinical context to upregulate *DHFR* expression[38]. The TMP-3 culture, the only one that acquired the –9G>A promoter mutation, had a genomic amplification spanning the *DHFR* gene (**Supplementary Fig. 1**). Mutations in the coding region (P21L, A26T, A26V, A26S, L28R, W30C, W30G, W30R and I94L) occur close to the substrate-binding site of DHFR (Asp27)[7,8,38–40], and all are known or predicted to have effects on DHFR enzymatic activity (**Supplementary Table 2**)[6–8,18,40]. Among these alterations, three (the –35C>T promoter mutation and the encoded P21L and W30R amino acid substitutions) were found in clinical isolates[18,38], four (P21L, A26T, W30R and I94L) were reported in laboratory selection[41], and four (the –35C>T and –9G>A promoter mutations and the L28R and W30C amino acid substitutions) appeared in independent selection experiments we performed on agar plates (**Supplementary Note** and **Supplementary Table 3**). The independent recurrence of the exact same nucleotide changes in replicate populations (13 recurrent mutations in trimethoprim compared to 2 in chloramphenicol and 1 in doxycycline), which may depend on the similarity of the selection pressure in these parallel populations, suggest a smaller genomic region in which mutations lead to trimethoprim resistance relative to the other drugs, consistent with the stepwise nature of the phenotypic adaptation to trimethoprim (**Fig. 2b**). The recurrent emergence of the same genotypic changes in independently evolving populations raises the question of whether the order in which these mutations emerge is also tightly constrained and not only their presence[1,6,42].

To determine the order of fixation of mutations during the evolution of trimethoprim resistance, we sequenced the *DHFR* locus of four random clones derived from the daily samples of parallel evolving populations (Online Methods). We found that the appearance and fixation of mutations were mostly sequential (**Fig. 4**), although we observed several exceptions in which two different mutations appeared simultaneously in competing clones in the population (clonal interference; **Supplementary Note**)[43]. The evolutionary trajectories shared striking similarities (**Fig. 4b**): all accumulated four *DHFR* mutations, all had a promoter mutation and, in each case, the final mutation affected the codon for Ala26 (A26T, A26V and A26S). Also, two populations (TMP-1 and TMP-2) accumulated exactly the same *DHFR* mutations (the –35C>T promoter mutation and those encoding P21L, L28R and A26T amino acid substitutions) in precisely the same order. Comparing our experimental results to a null random permutation model, we found that the ordered nature of the acquisition of these mutations was very unlikely to have occurred by chance ($P = 0.002$; **Fig. 4c** and Online Methods).

We conclude that the evolution of resistance to trimethoprim proceeds through the sequential fixation of mutations in a target enzyme through ordered pathways. The observation of constrained evolutionary trajectories for drug resistance is consistent with earlier predictions based on phenotypic measurements of bacteria with synthetically engineered intermediate genotypes for drug resistance alleles[1,6]. Our study is one of the first to directly show ordered adaptive pathways leading to high levels of antibiotic resistance in bacteria, complementing previous observations of the parallel evolution of virus populations[44,45]. Future studies with greater numbers of parallel evolving cultures are needed to identify additional paths to resistance and determine how such paths depend on the environment, population size and strength of selection pressure.

URLs. Mutation Assessor tool, http://mutationassessor.org.

METHODS

Methods and any associated references are available in the online version of the paper at http://www.nature.com/naturegenetics/.

Accession numbers. Whole-genome sequencing data from the morbidostat-evolved strains have been deposited in the NCBI Sequence Read Archive (SRA046097). Sample accessions numbers are provided in the **Supplementary Note**.

Note: Supplementary information is available on the Nature Genetics website.

ACKNOWLEDGMENTS

The authors thank M. Baym, S. Bershtein, T. Bollenbach, M. Ernebjerg, Y. Gerardin, J. Horn, A. Kocabas, C. Kocabas, D. Landgraf, R. Milo, B. Okumus, A. Palmer, J.M. Pedraza, M. Shuman, I. Wapinski, R. Ward, P. Yeh and all members of the Kishony laboratory for technical help and discussions. This work was supported in part by grants from the US National Institutes of Health (GM081617 to R.K. and GM079536 to D.L.H.) and The New England Regional Center of Excellence for Biodefense and Emerging Infectious Diseases (AI057159 to R.K.). J.-B.M. is supported by a Foundational Questions in Evolutionary Biology Fellowship.

AUTHOR CONTRIBUTIONS

E.T., A.V., R.C., D.L.H. and R.K. designed the project. E.T. and A.V. performed the experiments and E.T., A.V., J.-B.M. and R.K. analyzed the data. All authors contributed to preparing the manuscript.

COMPETING FINANCIAL INTERESTS

The authors declare no competing financial interests.

Published online at http://www.nature.com/naturegenetics/.
Reprints and permissions information is available online at http://www.nature.com/reprints/index.html.

1. Weinreich, D.M., Delaney, N.F., Depristo, M.A. & Hartl, D.L. Darwinian evolution can follow only very few mutational paths to fitter proteins. *Science* **312**, 111–114 (2006).
2. Bryson, V. & Szybalski, W. Microbial selection. *Science* **116**, 45–51 (1952).
3. Lee, H.H., Molla, M.N., Cantor, C.R. & Collins, J.J. Bacterial charity work leads to population-wide resistance. *Nature* **467**, 82–85 (2010).
4. Zhang, Q. *et al.* Acceleration of emergence of bacterial antibiotic resistance in connected microenvironments. *Science* **333**, 1764–1767 (2011).
5. Lane, P.G., Hutter, A., Oliver, S.G. & Butler, P.R. Selection of microbial mutants tolerant to extreme environmental stress using continuous culture-control design. *Biotechnol. Prog.* **15**, 1115–1124 (1999).
6. Lozovsky, E.R. *et al.* Stepwise acquisition of pyrimethamine resistance in the malaria parasite. *Proc. Natl. Acad. Sci. USA* **106**, 12025–12030 (2009).
7. Matthews, D.A. *et al.* Dihydrofolate reductase: x-ray structure of the binary complex with methotrexate. *Science* **197**, 452–455 (1977).
8. Schnell, J.R., Dyson, H.J. & Wright, P.E. Structure, dynamics, and catalytic function of dihydrofolate reductase. *Annu. Rev. Biophys. Biomol. Struct.* **33**, 119–140 (2004).
9. Couñago, R., Chen, S. & Shamoo, Y. *In vivo* molecular evolution reveals biophysical origins of organismal fitness. *Mol. Cell* **22**, 441–449 (2006).
10. Taubes, G. The bacteria fight back. *Science* **321**, 356–361 (2008).
11. Lipsitch, M., Bergstrom, C.T. & Levin, B.R. The epidemiology of antibiotic resistance in hospitals: paradoxes and prescriptions. *Proc. Natl. Acad. Sci. USA* **97**, 1938–1943 (2000).
12. Levy, S.B. & Marshall, B. Antibacterial resistance worldwide: causes, challenges and responses. *Nat. Med.* **10**, S122–S129 (2004).
13. Martinez, J.L. *et al.* A global view of antibiotic resistance. *FEMS Microbiol. Rev.* **33**, 44–65 (2009).
14. Davies, J. & Davies, D. Origins and evolution of antibiotic resistance. *Microbiol. Mol. Biol. Rev.* **74**, 417–433 (2010).
15. Yee, Y.C., Kisslinger, B., Yu, V.L. & Jin, D.J. A mechanism of rifamycin inhibition and resistance in *Pseudomonas aeruginosa*. *J. Antimicrob. Chemother.* **38**, 133–137 (1996).
16. Ruiz, J. Mechanisms of resistance to quinolones: target alterations, decreased accumulation and DNA gyrase protection. *J. Antimicrob. Chemother.* **51**, 1109–1117 (2003).
17. Chopra, I. & Roberts, M. Tetracycline antibiotics: mode of action, applications, molecular biology, and epidemiology of bacterial resistance. *Microbiol. Mol. Biol. Rev.* **65**, 232–260 (2001).
18. Huovinen, P. Trimethoprim resistance. *Antimicrob. Agents Chemother.* **31**, 1451–1456 (1987).
19. Girgis, H.S., Hottes, A.K. & Tavazoie, S. Genetic architecture of intrinsic antibiotic susceptibility. *PLoS ONE* **4**, e5629 (2009).
20. Albert, T.J. *et al.* Mutation discovery in bacterial genomes: metronidazole resistance in *Helicobacter pylori*. *Nat. Methods* **2**, 951–953 (2005).
21. Friedman, L., Alder, J.D. & Silverman, J.A. Genetic changes that correlate with reduced susceptibility to daptomycin in *Staphylococcus aureus*. *Antimicrob. Agents Chemother.* **50**, 2137–2145 (2006).
22. Barrick, J.E. *et al.* Genome evolution and adaptation in a long-term experiment with *Escherichia coli*. *Nature* **461**, 1243–1247 (2009).
23. Yeh, P.J., Hegreness, M.J., Aiden, A.P. & Kishony, R. Drug interactions and the evolution of antibiotic resistance. *Nat. Rev. Microbiol.* **7**, 460–466 (2009).
24. Michel, J.B., Yeh, P.J., Chait, R., Moellering, R.C. Jr. & Kishony, R. Drug interactions modulate the potential for evolution of resistance. *Proc. Natl. Acad. Sci. USA* **105**, 14918–14923 (2008).
25. Demerec, M. Production of Staphylococcus strains resistant to various concentrations of penicillin. *Proc. Natl. Acad. Sci. USA* **31**, 16–24 (1945).
26. Drlica, K. The mutant selection window and antimicrobial resistance. *J. Antimicrob. Chemother.* **52**, 11–17 (2003).
27. Bull, A.T. The renaissance of continuous culture in the post-genomics age. *J. Ind. Microbiol. Biotechnol.* **37**, 993–1021 (2010).
28. de Crécy, E. *et al.* Development of a novel continuous culture device for experimental evolution of bacterial populations. *Appl. Microbiol. Biotechnol.* **77**, 489–496 (2007).
29. Paalme, T., Elken, R., Kahru, A., Vanatalu, K. & Vilu, R. The growth rate control in *Escherichia coli* at near to maximum growth rates: the A-stat approach. *Antonie van Leeuwenhoek* **71**, 217–230 (1997).
30. Yeh, P., Tschumi, A.I. & Kishony, R. Functional classification of drugs by properties of their pairwise interactions. *Nat. Genet.* **38**, 489–494 (2006).
31. Arjan, J.A. *et al.* Diminishing returns from mutation supply rate in asexual populations. *Science* **283**, 404–406 (1999).
32. Okusu, H., Ma, D. & Nikaido, H. AcrAB efflux pump plays a major role in the antibiotic resistance phenotype of *Escherichia coli* multiple-antibiotic-resistance (Mar) mutants. *J. Bacteriol.* **178**, 306–308 (1996).
33. Asako, H., Nakajima, H., Kobayashi, K., Kobayashi, M. & Aono, R. Organic solvent tolerance and antibiotic resistance increased by overexpression of marA in *Escherichia coli*. *Appl. Environ. Microbiol.* **63**, 1428–1433 (1997).
34. Mankin, A.S., Zyrianova, I.M., Kagramanova, V.K. & Garrett, R.A. Introducing mutations into the single-copy chromosomal 23S rRNA gene of the archaeon *Halobacterium halobium* by using an rRNA operon-based transformation system. *Proc. Natl. Acad. Sci. USA* **89**, 6535–6539 (1992).
35. Gerrits, M.M., Berning, M., Van Vliet, A.H., Kuipers, E.J. & Kusters, J.G. Effects of 16S rRNA gene mutations on tetracycline resistance in *Helicobacter pylori*. *Antimicrob. Agents Chemother.* **47**, 2984–2986 (2003).
36. Ross, J.I., Eady, E.A., Cove, J.H. & Cunliffe, W.J. 16S rRNA mutation associated with tetracycline resistance in a gram-positive bacterium. *Antimicrob. Agents Chemother.* **42**, 1702–1705 (1998).
37. Ettayebi, M., Prasad, S.M. & Morgan, E.A. Chloramphenicol-erythromycin resistance mutations in a 23S rRNA gene of *Escherichia coli*. *J. Bacteriol.* **162**, 551–557 (1985).
38. Flensburg, J. & Skold, O. Massive overproduction of dihydrofolate reductase in bacteria as a response to the use of trimethoprim. *Eur. J. Biochem.* **162**, 473–476 (1987).
39. Ohmae, E., Sasaki, Y. & Gekko, K. Effects of five-tryptophan mutations on structure, stability and function of *Escherichia coli* dihydrofolate reductase. *J. Biochem.* **130**, 439–447 (2001).
40. Smith, D.R. & Calvo, J.M. Nucleotide sequence of dihydrofolate reductase genes from trimethoprim-resistant mutants of *Escherichia coli*. Evidence that dihydrofolate reductase interacts with another essential gene product. *Mol. Gen. Genet.* **187**, 72–78 (1982).
41. Watson, M., Liu, J.W. & Ollis, D. Directed evolution of trimethoprim resistance in *Escherichia coli*. *FEBS J.* **274**, 2661–2671 (2007).
42. Lunzer, M., Miller, S.P., Felsheim, R. & Dean, A.M. The biochemical architecture of an ancient adaptive landscape. *Science* **310**, 499–501 (2005).
43. de Visser, J.A. & Rozen, D.E. Clonal interference and the periodic selection of new beneficial mutations in *Escherichia coli*. *Genetics* **172**, 2093–2100 (2006).
44. Wichman, H.A., Badgett, M.R., Scott, L.A., Boulianne, C.M. & Bull, J.J. Different trajectories of parallel evolution during viral adaptation. *Science* **285**, 422–424 (1999).
45. Crandall, K.A., Kelsey, C.R., Imamichi, H., Lane, H.C. & Salzman, N.P. Parallel evolution of drug resistance in HIV: failure of nonsynonymous/synonymous substitution rate ratio to detect selection. *Mol. Biol. Evol.* **16**, 372–382 (1999).

ONLINE METHODS

Bacterial strains, media and growth conditions. All experiments were performed with the drug-sensitive, wild-type MG1655 *E. coli* strain. Cells were grown at 30 °C in sterile M9 minimal medium supplemented with 0.4% glucose and 0.2% amicase (Sigma).

Morbidostat schematics and protocol details. Detailed information on the morbidostat schematics, construction and calibration, as well as a complete description of the experimental procedure can be found in the **Supplementary Note** and in **Supplementary Figure 2**.

Dilution rate in the morbidostat. Dilution rate was calculated by $r_{dilution} = f \cdot \ln(V/(V + \Delta V))$, where f is the frequency of dilutions in an hour (f = 5), V is the total volume of the culture before the dilution ($V \approx 12$ ml) and V is the added volume per injection ($\Delta V \approx 1$ ml). With these settings, $r_{dilution}$ is ~0.4 h^{-1}.

Growth rate in the morbidostat. All of the experiments were carried out at 30 °C in M9 minimal medium supplemented with 0.4% glucose and 0.2% amicase. Growth medium was filter sterilized and kept at room temperature for 2 d on the bench before using in the experiments to avoid contamination. We characterized bacterial growth under these conditions by growing *E. coli* cells for 12 h (**Supplementary Fig. 2e**). The cells grew in exponential phase when the OD was between 0.02 and 0.25, and the exponential growth rate was ~0.8 h^{-1} (**Supplementary Fig. 2e**, red line). The growth rate variability (s.d.) across all 15 cultures was 7.5%.

Whole-genome sequencing. Isogenic bacterial cells were grown overnight in LB medium, and their chromosomal DNA was purified using commercial bacterial DNA isolation kits (UltraClean Microbial DNA Isolation Kit; 12224-50, MO BIO Laboratories). Chromosomal DNA libraries were prepared for Illumina sequencing using DNA sample prep kits (Nextera DNA Sample Prep Kit; GA091120, EPICENTRE Biotechnologies). Chromosomal DNA libraries were submitted to Partners HealthCare Center for Personalized Genetic Medicine (PCPGM) for whole-genome sequencing on an Illumina Gene Analyzer IIx (75-bp single-end reads, average coverage of 6 million reads per strain). These reads were then aligned onto the MG1655 reference chromosome (NC_000913.2) using the Illumina pipeline, and putative SNPs were identified with SAMtools[46].

Sanger sequencing protocol. Sanger sequencing was used to verify high-confidence SNPs (SAMtools threshold >60) found with Illumina sequencing. Isogenic bacterial populations frozen in 15% glycerol were sent for sequencing to GENEWIZ, from whom primer design, PCR quality control, amplification and sequencing services were commercially available. Every locus was sequenced in both directions, with fragments of approximately 400 bp insuring high-quality reads over the region containing the SNPs, and sequence quality was verified by manual inspection. The complete list of confirmed SNPs and their predicted effects is provided in **Supplementary Table 2**.

Functional consequences of mutations. The functional impact of individual mutations was predicted using the online Mutation Assessor tool (see URLs) available from the Computational Biology Center of the Memorial Sloan-Kettering Cancer Center[47]. The Mutation Assessor tool uses multiple sequence alignments of related genes in other organisms to determine the functional impact of a specific mutation. This functional impact of the SNP is scored on the basis of the conservation and specificity of the position. The predicted functional impact scores of the confirmed SNPs are listed in **Supplementary Table 2**.

Reproducibility of mutational order. We devised a statistical method to assess the probability of observing the order at which mutations occurred in five populations by random chance. We define the reproducibility of mutational order (RMO) score of two ordered sequences of mutations by the number of shared mutation pairs that occurred in the same order, from which we subtract the number of shared mutation pairs that occurred in reverse order. (For example, RMO ([A,B,C,D], [A,X,C,B]) = 2 − 1 = 1, as two shared mutation pairs occurred in the same order, [A,B] and [A,C], but one shared mutation pair occurred in the opposite order, [B,C] and [C,B].) The RMO for the set of five populations we observed is 22 (summing the RMOs of all 10 distinct pairs of sequences). The highest possible total RMO score for five populations acquiring four of the six mutations we observed is 28. A random permutation of the order at which mutations appear in those five populations produced an equally high RMO in less than 200 cases out of 100,000 iterations (**Fig. 4c**), yielding a P value of 0.002 that characterizes the probability that the observed degree of ordering of mutations is produced by chance. We also repeated the same test, generating five trajectories by randomly selecting four mutations from the pool of six observed mutations. In this case, we found that only 0.073% of randomly generated trajectories are equally or more ordered that the experimentally observed trajectories.

Phenotyping protocol. We created a frozen record library in order to measure phenotypic and genotypic changes with high temporal resolution. On a daily basis, cells were frozen and stored at −80 °C in 15% glycerol. These samples were organized in 96-well plates. We measured the drug resistance of these libraries using an automated robotic system (Caliper). First, we filled 20 such plates with drug solutions (in minimal growth medium) with increasing drug concentrations. Each well in a given plate had the same volume (150 µl) and drug concentration. The first plate had the highest drug concentration and the twentieth plate was drug free. Drug concentrations across the other plates were diluted by a factor of 0.6 ($[drug]_{k-1} = 0.6 \times [drug]_k$). The cells in master plates were transferred into experimental plates using a 96-pinner. Cells in 96-well plates were grown for 24 h in an environment-controlled room with rapid shaking at 30 °C. Optical densities of the cells were measured approximately every 30 min using a plate reader (EnVision; Perkin Elmer).

Calculating MIC and IC_{50}. OD reads from the plates used in the phenotyping experiment were used to calculate the IC_{50} and MIC values of the evolving strains. For every well in every plate, the growth rate during the exponential phase was measured by fitting an exponential curve to the region of the data points in which the OD was between 0.01 and 0.1. For each strain within the frozen record library, the calculated growth rates were used to produce dose-response curves (**Supplementary Fig. 3**). These dose-response curves reflect the effect of increasing concentrations of antibiotics on the strains' growth rates. For IC_{50} and MIC analysis, the growth rates were normalized using the growth rate in the no-drug condition. The IC_{50} and MIC values were calculated by interpolating the drug concentrations corresponding to growth rates of 50% and 10%, respectively (**Supplementary Fig. 3**).

Measuring static MIC for isogenic cells. We repeated the same protocol to measure the MIC of single colonies from each population. We plated cells from the frozen record library and randomly picked single colonies for every day of the experiment. These colonies were organized in 96-well plates and were grown in a range of different drug concentrations for 24 h. The lowest drug concentration at which background-subtracted OD was less than 0.02 after 24 h was defined as the MIC[48]. All of the evolved strains were tested for their MIC values for chloramphenicol, doxycycline and trimethoprim.

Calculating dynamic IC_{50}. For every cycle during the morbidostat experiment, we fit an exponential growth curve to the OD versus time data using Matlab's robust fit linear regression. Using the exponential growth regressions, we calculated the initial and final OD for each cycle. By calculating the ratio of the final and initial ODs of successive cycles, we determined the precise dilution that occurred in the culture tube between the cycles. These dilutions were sparsely spread around the target dilution rate of 8%. Given the dilution factor and the knowledge of which stock solution (medium, low-concentration drug stock or high-concentration drug stock) was used, we calculated for every cycle the antibiotic concentration in the culture tube. We plotted the growth rate as a function of drug concentration and produced drug-response curves as shown in **Supplementary Figure 4**. A curve was produced for each time period between drug injections. During this time window, we calculated the population's dynamic IC_{50} by finding the drug concentration at which the resulting growth rate was 0.4 h^{-1}.

Selection of trimethoprim-resistant mutants on agar plates. Agar plates (1.5% agar, M9 salts, 0.2% amicase and 0.4% glucose) without drug and with 15 different trimethoprim concentrations (1,500 to 0.18 µg/ml, in 1:2 dilutions) were prepared in sterile conditions. Cells (~1×10^9) were spread on each plate and plates were incubated at 30 °C for 3 d. Colony-forming units were then picked, restreaked to isolation and sequenced.

46. Li, H. *et al.* The Sequence Alignment/Map format and SAMtools. *Bioinformatics* **25**, 2078–2079 (2009).
47. Reva, B., Antipin, Y. & Sander, C. Determinants of protein function revealed by combinatorial entropy optimization. *Genome Biol.* **8**, R232 (2007).
48. Bollenbach, T., Quan, S., Chait, R. & Kishony, R. Nonoptimal microbial response to antibiotics underlies suppressive drug interactions. *Cell* **139**, 707–718 (2009).

doi:10.1038/ng.1034